Volume 10, Issue 4, 2020, 5951 - 5959 ISSN 2069-5837

Biointerface Research in Applied Chemistry

www.BiointerfaceResearch.com

https://doi.org/10.33263/BRIAC104.951959

Original Research Article Open Access Journal

Received: 03.04.2020 / Revised: 20.04.2020 / Accepted: 20.04.2020 / Published on-line: 23.04.2020

The activation energy and antibacterial investigation of spherical Fe_3O_4 nanoparticles prepared by *Crocus sativus* (Saffron) flowers

Shashanka Rajendrachari [*1], Kevser Betül Ceylan [2]

[1]Department of Metallurgical and Materials Engineering, Bartin University, Bartin-74100, Turkey
[2]Department of Molecular Biology and Genetics, Faculty of Science, Bartin University, Bartin, Turkey
*corresponding author e-mail address: ***shashankaic@gmail.com*** | Scopus ID 55851104900

ABSTRACT

We proposed a simple and environmental-friendly method to prepare magnetite nanoparticles and their application as antibacterial material. We successfully prepared Fe_3O_4 nanoparticles using *Crocus Sativus* (Saffron) flowers followed by calcination at 400 ˚C for 15 minutes. The UV–Visible spectroscopy was used to study the bandgap energy of the prepared Fe_3O_4 nanoparticles and the value was found to be 3.23 eV. The scanning electron microscopy (SEM) was used to study the structure and morphology and X-ray diffraction was used to study the phase and crystallite size of the magnetite nanoparticles. The percentage weight loss, the enthalpy change and activation energy of Fe_3O_4 nanoparticles were calculated by using the thermogravimetric (TG) and differential thermal analysis (DTA) respectively. The DTA curve at a heating rate of 6, 8 and 10˚C/min shows endothermic peaks at 586, 594 and 600˚C respectively. The activation energy of Fe_3O_4 nanoparticles was calculated by the Kissinger method and was found to be 8.09 kJ/moles. The antibacterial activity of Fe_3O_4 nanoparticles was carried out against 3 gram-positive and 3 gram-negative bacteria by using a minimum inhibition concentration (MIC) assay method and they showed excellent antibacterial activity against gram-negative bacterial strains only. **Keywords:** *Antibacterial activity; Fe_3O_4 nanoparticles; Crocus Sativus; saffron flower extract; activation energy:*

1. INTRODUCTION

Nanotechnology is now universally considered as the potential research topic that can benefit the different fields such as biomedical, chemical, physical, civil, mechanical, metallurgical and materials engineering [1-6]. Nanomaterials had brought significant improvement in drug delivery, water purification, sensors, development of lighter alloys, composites, information and communication technologies, etc. Using nanotechnology one can easily create and manipulate the materials with different properties, either by scaling up from single groups of atoms or by the refining of bulk materials [7, 8].

The recent past has witnessed a variety of nanomaterials like graphene, fullerenes, metal nanoparticles, metal oxide nanoparticles, carbon nanotubes, nanoalloys, etc. All these nanomaterials exhibit a wide range of properties as well as applications; but among all, the metal oxide nanoparticles are one of the conventional types of nanomaterials advancing with rocket speed due to the ease of production. The extremely refined size, maximum surface area, excellent physical, biological, chemical, and mechanical properties had made metal oxide nanoparticles one of the very important nanomaterials [9].

The metal oxide nanoparticles like Fe_3O_4 nanoparticles have shown tremendous potential in designing advanced functional materials in chemical and biomedical fields. They also exhibit very interesting properties like superparamagnetic properties [10], biocompatibility, pigmentation, biodegradability, non-toxic nature, etc. [11–13]. Due to their wide range of properties they can be exploited to design new bio-diagnostic, therapeutic strategies, innovative biotechnology methodologies and can also be used as a material for catalysis (for carbon nanotube production) [14-16], magnetic storage media [17], biosensors [18], magnetic resonance imaging contrast agents [19-21], targeted drug delivery [22–24], nickel-iron batteries and as sorbents for environmental remediation [21, 25]. Therefore, over the last few years, magnetite nanoparticles have been the hot topic among the chemical, biological and material researchers. But, control over their size, shape, and composition is still a challenging part for the researchers; without achieving them one cannot use them in a complex biological system to revolutionize the medical field. Therefore, we are reporting a simple method to prepare Fe_3O_4 nanoparticles with strong control over their size, shape, and composition.

Many researchers have reported the synthesis of Fe_3O_4 nanoparticles by various methods like reverse micelle [26-29], copolymer template method [26, 30, 31], co-precipitation [32], sol-gel method [33], electrochemical method [34], solvothermal method [35] and hydrothermal [36] methods, etc. But these methods are tedious, slow, expensive and may require some special equipment, capping agents, high temperature and templates (result in impurities), etc. Most of these methods require strong toxic chemicals; which are very dangerous to the environment. Therefore, in the present paper, we reported a simple, rapid, inexpensive, non-toxic and eco-friendly route to prepared Fe_3O_4 nanoparticles using *Crocus Sativus (Saffron) flowers* extract. The shape, size, and composition of the iron oxide nanoparticles can be easily controlled using this method just by maintaining the proper pH, solvent concentration, pressure and experimental temperature [37].

Crocus Sativus is also called *saffron crocus*, or *autumn crocus* as reported by the United States Department of Agriculture and this flowering plant belongs to the iris family Iridaceae [38].

The spice saffron can be produced from the filaments that grow inside the *Crocus Sativus* flower. They are generally found in the Mediterranean, Eastern Greece, East Asia, and Irano-Turanian Region [39-41]. Saffron is considered to be one of the most valuable spice by weight [39] and is sometimes toxic if we intake excess [42]. The phytochemicals present in *Crocus Sativus* itself acts as capping agent as well as reducing agent and reduces the agglomeration and eventually reduces the iron salt to iron oxide.

Clarina *et al*. prepared magnetite nanoparticles using *Polpala* flower extract and characterized by UV-Vis absorbance spectroscopy, FT-IR spectroscopy, XRD and SEM [43]. They found the average particle size of 38 nm with highly crystalline iron oxide nanoparticles. They reported the potential applications of prepared magnetite nanoparticles in biomedical and recyclable magnetic nano-catalyst for organic reactions [43].

Karpagavinayagam *et al*. described a non-hazardous method for preparing iron oxide nanoparticles using *Avicennia marina* flower extract. They studied the absorption spectrum, morphology, and electrochemical properties. They reported that the prepared iron oxide nanoparticles can be used in industrial, dye degradation and control the environment pollution [44].

Sari *et al*. prepared magnetite (Fe_3O_4) nanoparticles using *Graptophyllum pictum* leaf extract. They reported that the presence of phytochemicals acts as a capping agent and reducing agent [45]. Ramesh *et al*. reported the green synthesis of Fe_3O_4 nanoparticles using *Zanthoxylum armatum* aqueous leaf extract. They successfully used prepared magnetite nanoparticles for efficient adsorption of organic pollutants, methylene blue [46].

One of the important advantages of the reported method is the huge availability of flora on the earth and the presence of phytochemicals like aldehydes, ketones, flavonoids, and phenols in the plant extract. They act as reducing agents, capping agents and converts metal salts into metal oxide nanoparticles [47]. The presence of flavonoids and phenols in the plants improve their antioxidant antibacterial properties [48]. Karimi *et al*. [49] reported that *Crocus Sativus* contains 6.54 ± 0.02 mg gallic acid equivalent (GAE)/g dry weight (DW) phenolic contents, 5.88 ± 0.12 mg rutin equivalent/g dry weight of total flavonoids. Due to the presence of more amount of phenolic and flavonoid groups in *Crocus Sativus*, we have decided to prepare iron oxide nanoparticles from them. This method is one of the simple, low cost, robust, nontoxic and eco-friendly method to prepare Fe_3O_4 nanoparticles. Many researchers have reported a green synthesis of magnetite nanoparticles by various plant extracts, but no literature is available on the green synthesis of magnetite nanoparticles using *Crocus Sativus* flowers. Therefore, we reported the preparation of Fe_3O_4 nanoparticles by using *Crocus Sativus* (Saffron) flowers and their antibacterial activities.

2. MATERIALS AND METHODS

2.1. Chemicals and reagents required.

Iron (III) Chloride Hexahydrate [$FeCl_3.6H_2O$], Iron (II) Chloride Tetrahydrate [$FeCl_2.4H_2O$], Sodium hydroxide (NaOH) of Sigma-Aldrich brand was purchased from Umay laboratuvar, Istanbul, Turkey. *Crocus Sativus* (Saffron) flower extract was prepared in the lab and all the solutions were prepared by using double distilled water.

2.2. Preparation of flower extract.

The fresh *Crocus Sativus* (Saffron) flowers were collected from the market of Safranbolu, Turkey with the help of an expert from Bartin University, Turkey and were washed thoroughly using double distilled water. Two grams of the fresh *Crocus Sativus* (Saffron) flowers were cut into small pieces and then added 100 mL of deionized water. Further, the solution was boiled around 80 ˚C for 15 to 20 minutes until we get a strong red-colored solution and cool the solution to room temperature (around 25 ˚C). Filter the flower extract solution using general-purpose filter paper followed by centrifugation to remove any impurities to get a clear red colored solution.

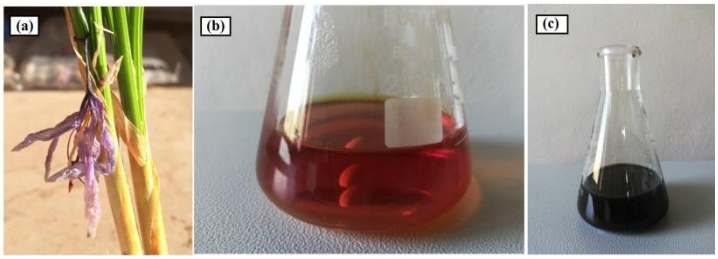

Figure 1. (a) Crocus Sativus (Saffron) flowers (b) Saffron flower extract (c) Colloidal solution of Fe_3O_4 nanoparticles

A small quantity of the flower extract was used all the time during the experiment to prepare magnetite nanoparticles and remaining aliquots of flower extract was stored at 5 ˚C temperature for further use. Figure 1 shows the *Crocus Sativus* (Saffron) flowers, its extract and colloidal solution of Fe_3O_4 nanoparticles.

2.3. Preparation of Fe_3O_4 nanoparticles.

Dissolve 2 grams of Iron (II) Chloride Tetrahydrate and 1 gram of Iron (III) Chloride Hexahydrate powders in 100 mL of deionized water. The solution was stirred on a magnetic stirrer for 10 minutes at 80 ˚C to get a homogeneous yellow colored solution.

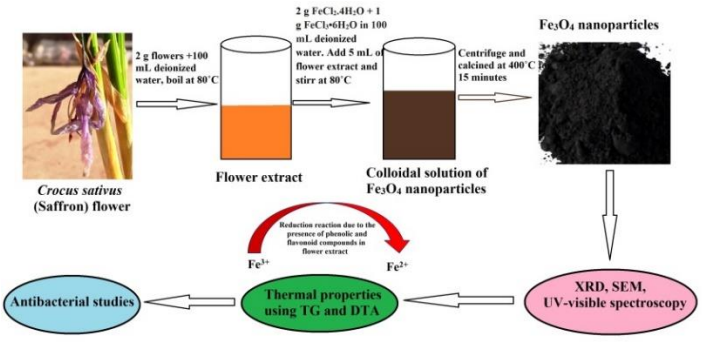

Figure 2. Schematic representation of the preparation of Fe_3O_4 nanoparticles from *Crocus Sativus* (Saffron) flowers

Later added 5 mL of red-colored *Crocus Sativus* (Saffron) flower extract slowly into the iron salt solution. Then the entire solution turns from yellow color to dark brownish color indicating the initial generation of magnetite nanoparticles and continues the heating and stirring for 10 minutes to get a homogeneous solution. Further, 0.1 M NaOH solution was added dropwise (for 10 minutes) to precipitate all the Fe_3O_4 nanoparticles from the black colored solution. Then the solution was allowed to cool down to room temperature and centrifuged for 10 minutes at 7500 rpm to remove all the impurities by removing the supernatant solution. Washed the magnetite nanoparticles 3 times using distilled water followed by centrifugation. The dark black colored Fe_3O_4 nanoparticles were

dried on a watch glass at 70 ˚C in a laboratory oven for 1 day. The dried black colored Fe_3O_4 nanoparticles were later calcined in a furnace at 400 ˚C for 15 minutes to remove any volatile impurities. The calcined samples were then cooled to room temperature, pulverized and then stored for further characterization.

Figure 2 shows the schematic representation of preparing Fe_3O_4 nanoparticles using *Crocus Sativus* (Saffron) flower extract. This plant extract acts as both reducing agents as well as capping agents in preparing Fe_3O_4 nanoparticles due to the presence of phenolic and flavonoid compounds like gallic acid, pyrogallol, β-carotene, lycopene, vitamin E, ascorbic acid [49]. Siddhuraju and Becker [50] have reported that, as the phenolic and flavonoid levels increase the reducing power of the plant will also increase. Karimi *et al*. [49] also reported the ferric reducing power activity of *Crocus Sativus* (Saffron) flowers and they concluded that it can strongly reduce Fe^{3+} to Fe^{2+}.

2.4.Characterization of Fe_3O_4 nanoparticles.

XRD (RIGAKU SmartLab) was used to study the phases of prepared Fe_3O_4 nanoparticles with the 2θ range between 20-80˚ using Cu $Ka_{\alpha 1}$ radiation (λ=1.54056 Å). The morphology of the nanoparticles was investigated by using SEM (TESCAN- MAIA3 XMU) and their quantitative analysis was carried out by using energy dispersive spectroscopy (EDS) attached to SEM. UV-Visible spectroscopy (Shimadzu- UV 3600 Plus) was used to study the optical properties of magnetite nanoparticles respectively. Hitachi, STA 7300 model was used to studying the thermal properties. Antibacterial activities of the prepared magnetite (Fe_3O_4) nanoparticles were studied by using gram-negative and gram-positive bacteria by the MIC assay method.

2.5. Antibacterial activity.

Three gram-positive (*Bacillus subtilis, Enterococcus faecalis, Staphylococcus aureus*) and gram-negative (*Escherichia coli, Salmonella enteridis, Pseudomonas aeruginosa*) bacteria were tested to clarify the antibacterial effect of Fe_3O_4 nanoparticles composed of saffron. Whole bacteria were procured by the Department of Molecular Biology and Genetics of Bartın University (Bartin, Turkey). Minimum inhibition concentration (MIC) was described that the lowest concentration at which bacterial growth is inhibited under regular conditions [51]. The turbidity of the bacteria inoculated in LB medium was adjusted to 0.5 McFarland (1.5x108 CFU/ml). 100 µL MHB medium was added to 96 well plate and Fe_3O_4 nanoparticles at a concentration of 5 mg/mL were added on to first wells then 2 fold dilution applied until the lowest concentration of 0.3125 mg/mL. After bacterial inoculation, the microplate was incubated at 37 ˚C for overnight. Bacterial turbidity of the overnight grown plates was measured by UV-Visible spectrum at 600 nm. MIC value is the lowest concentration of any substance where no visible bacterial growth is detected [52]. In order to determine the minimum bactericidal concentrations (MBC) of the Fe_3O_4 nanoparticles, the wells with no growth or suspected bacterial growth were inoculated onto Petri dishes and incubated at 37 ˚C for 24 h. MIC is the lowest concentration required to inhibit bacterial growth. Minimum Bactericidal Concentration (MBC) assay determines the lowest concentration required to kill microorganisms.

3. RESULTS

3.1 X-Ray diffraction.

Figure 3 depicts the XRD diffraction pattern of magnetite nanoparticles prepared by *Crocus Sativus* (Saffron) flower extract. The diffraction peaks at 2θ of 30.33° and 35.74° correspond to (220) and (311) planes respectively and all the diffraction peaks were perfectly matched with the JCPDF Card No.: 01-073-9877.

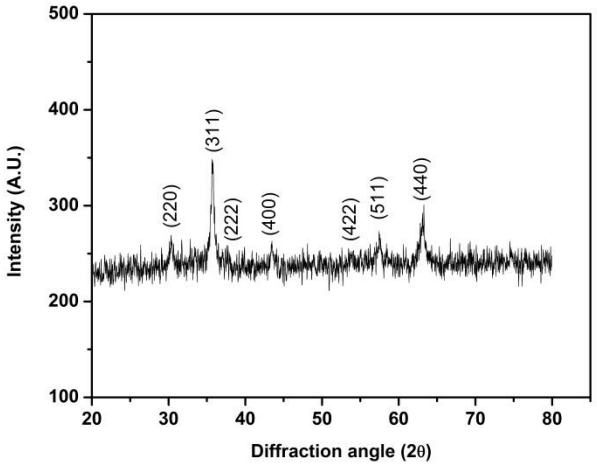

Figure 3. XRD diffraction spectra of Fe_3O_4 nanoparticles prepared by using *Crocus sativus* (Saffron) flower extract.

The diffraction peaks of prepared magnetite nanoparticles are broadened due to their nano-structure and exhibit cubic structure with space group Fd-3m(227).

Scherrer's formula [52, 53] was used to calculate the crystallite size of the prepared Fe_3O_4 nanoparticles as follows:

$$D = \frac{K\lambda}{\beta \cos\theta} \qquad (1)$$

Where, D= Average crystallite size, K= Constant equal to 0.94, λ= the wavelength of X-ray radiation (0.154 nm), β= Full-width half maximum of the peak (FWHM) (in radians) and 2θ= Bragg's angle (degree).

We have calculated the crystallite size for the 2 high-intensity peaks (220) and (311) using Scherrer's equation and the values were found to be ≈15 nm.

The nanoparticles with crystallite size less than 20 nm exhibit maximum strain than those nanoparticles whose crystallite size is more than 20 nm as reported by Aparna *et al*. [54]. Hence, according to Scherrer's equation, our magnetite nanoparticles are having an average crystallite size of 15 nm; therefore, our nanoparticles tend to have maximum strain. To study the lattice strain of the prepared magnetite nanoparticles in detail, we have used Williamson-Hall equation [55, 56] as follows;

$$\beta cos\theta = \frac{0.94\lambda}{D} + 4\varepsilon\, sin\theta \qquad (2)$$

Where 'β' is FWHM, 'ε' is the strain, 'D' is the average crystallite size and 'θ' is the Bragg's diffraction angle.

Williamson and Hall proposed a method for de-convoluting the size and strain broadening by looking at the peak width as a function of 2θ. Here, Williamson-Hall plot was plotted with sin θ on the x-axis and βcosθ on the y-axis (β in radians).

From the linear fit, particle size and strain were extracted from y-intercept and slope respectively [57-60]. According to the Williamson-Hall equation, the average crystallite size and lattice

strain of the magnetite nanoparticles were found to be ~12 nm and 0.29 respectively. Figure 4 depicts the Williamson-Hall Plot for Fe_3O_4 nanoparticles prepared by *Crocus Sativus* (Saffron) flowers. The peak intensities and positions are well-matched with the reported values.

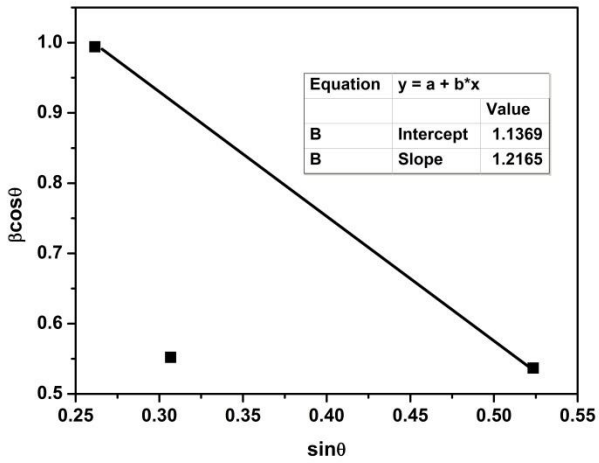

Figure 4. Williamson-Hall Plot for Fe_3O_4 nanoparticles.

3.2. Scanning electron microscopy.

Figure 5 (a) depicts the SEM image of Fe_3O_4 nanoparticles prepared from *Crocus Sativus* (Saffron) flower extract. Magnetite nanoparticles exhibit cubic and almost spherical structures with nearly equal to 25 nm particle size. The prepared nanoparticles were not agglomerated even though capping agents are not used [61]. The flower extract itself acts as a natural capping agent due to the presence of a large number of phytochemicals in the flower. The prepared flower extract also exhibits a strong reducing power due to the presence of more amount of phenolic and flavonoid compounds; as a result of which Fe^{3+} in the precursor reduced to Fe^{2+} effectively [49, 50]. Therefore, this method is very much environmentally friendly, simple and cost-effective.

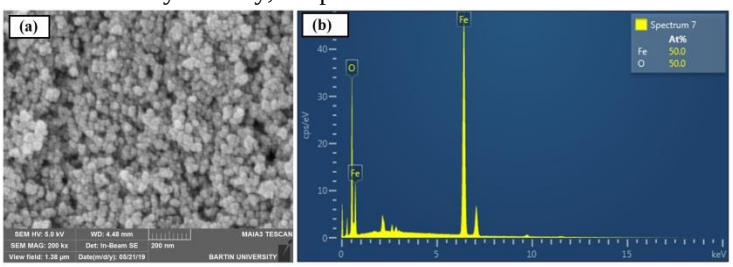

Figure 5. (a) SEM image of Fe_3O_4 nanoparticles **(b)** Energy dispersed spectroscopy (EDS) image of Fe_3O_4 nanoparticles prepared by *Crocus Sativus* (Saffron) flowers.

The qualitative and quantitative elemental analysis of prepared Fe_3O_4 nanoparticles were carried out using EDS. Figure 5 (b) represents the EDS image and elemental composition of magnetite nanoparticles prepared from *Crocus Sativus* (Saffron) flower extract. The atomic percentage of iron and oxygen was theoretically calculated as 50% each. Similarly, the experimental atomic percentage of copper and oxygen were found to be 50% each. Both iron and oxygen atoms present in prepared Fe_3O_4 nanoparticles are stoichiometric to each other and agree with the theoretical and experimental values.

3.3. UV-Visible spectroscopy.

The UV-Visible spectra of Fe_3O_4 nanoparticles prepared from *Crocus Sativus* (Saffron) flower extract are shown in figure 6. The prepared nanoparticles were dispersed in de-ionized water using an ultra sonicator for 2 minutes to get a homogeneous solution.

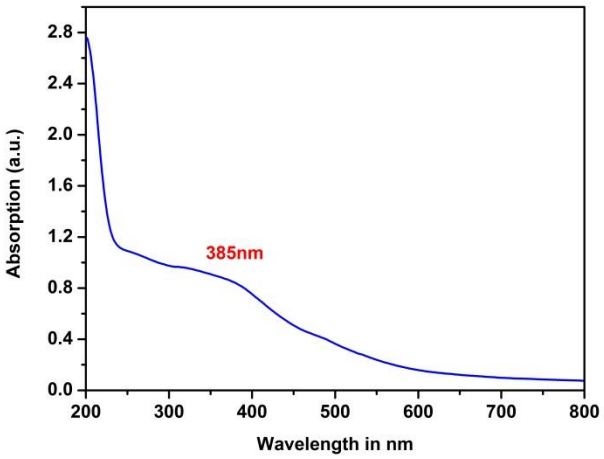

Figure 6. UV-Visible spectra of green synthesized Fe_3O_4 nanoparticles

Generally, UV-Visible spectroscopy uses light in the near-UV and near-infrared ranges and in this visible range molecules undergo electronic transitions and directly affect the perceived color of the chemicals involved [62]. The UV-visible spectrum shows a broad surface Plasmon resonance absorption peak at 385 nm. This surface plasmon resonance absorption phenomenon occurs due to the collective oscillation of the free conduction band electrons when electromagnetic radiation strikes them and incident light far exceeds the particle diameter [63]. The UV-visible spectrum does not show any other absorbance peaks, indicating the high purity of the prepared magnetite nanoparticles.

The bandgap energy (E) of the prepared magnetite nanoparticles were calculated by using the following equation;

$$E = \frac{h \times C}{\lambda} \qquad (3)$$

Where E = Bandgap energy

h = Planks constant = 6.626×10^{-34} Joules.sec

C = Speed of light = 3.0×10^{8} meter/sec

λ = Cut off wavelength = 385×10^{-9} meters

*Conversion $1eV = 1.6 \times 10^{-19}$ Joules

The calculated band gap energy of magnetite nanoparticles was found to be 3.23 eV. As band gap values decreases, the conductivity of the nanoparticles increases. Ghandoor *et al*. [64] reported the bandgap of magnetite nanoparticles as 3.64 eV, and Diasty *et al*. [65] reported the same as 5.7 eV. The prepared magnetite nanoparticles show fewer bandgap values than the reported values and hence more conductive in nature [66].

3.4. Thermal analysis.

The thermal properties of prepared magnetite nanoparticles were investigated by using thermogravimetric analysis (TG) and differential thermal analysis (DTA) over a temperature range of 30–1000 ˚C. Figures 7 (a), 7 (b) and 7 (c) represent the TG and DTA curves of Fe_3O_4 nanoparticles at 6, 8 and 10 ˚C/minute heating rates respectively.

The prepared Fe_3O_4 nanoparticles show good thermal stability over 30–1000˚C temperature range and exhibit less weight

loss. This is due to the significant resistance of Fe_3O_4 nanoparticles against evaporation and phase change at that temperature range. During a heating rate of 6˚C/min, only 2.8% weight loss was observed between 30 to 500˚C due to water evaporation, decomposition of organic material and carbonaceous matter [67] and nearly 1.3% weight loss was observed at 500–650˚C due to the phase transformation from Fe_3O_4 to FeO, as FeO is thermodynamically more stable above 570 ˚C according to the Fe-O phase diagram [68]. At higher temperatures, there is a possibility of deoxidation of FeO under the N_2 atmosphere as reported by S.Y Zhao *et al*. [69]. The total weight loss during heating rate 6˚C/min was found to be 4.6%. In the case of 8˚C/min, only 2.5% weight loss was observed between 30–500˚C due to the evaporation of water and 1.2% weight loss was observed over 500-650˚C due to the decomposition of organic material [70]. The total weight loss during 8˚C/min was found to be 4.4%. Similarly, during 10˚C/min, 4.4% weight loss was observed between 30–500˚C and the total weight loss was found to be 5.6%.

In another set of experiments, we studied the change in enthalpy and activation energy by using differential thermal analysis. The DTA curve at 6, 8 and 10 ˚C/min heating rates, we can observe endothermic peaks at 586, 594 and 600 ˚C respectively. These endothermic peaks confirm the decomposition of organic matter and carbonaceous materials, the phase transformation from Fe_3O_4 to FeO, and the deoxidation of FeO, respectively. The enthalpy change of prepared magnetite nanoparticles at 6, 8 and 10 ˚C/min heating rates were found to be 2.2, 3.57 and 6.64 kJ/mol respectively. From the DTA curves, it was observed that, as the heating rate increases from 6-10 ˚C/min, the maxima of the endothermic peak shift towards higher temperatures. This is due to the variation of enthalpy change as well as the temperature of the end of transition at higher heating rates [71]. The calculated details of weight loss, decomposition peak temperature, enthalpy change Fe_3O_4 nanoparticles prepared from *Crocus Sativus* (Saffron) flower extract are tabulated in table 1.

Table 1. The calculated details of weight loss, endothermic peak temperature, enthalpy change of prepared Fe_3O_4 nanoparticles using TG and DTA curves.

Type of nanomaterial	Heating rate (°C /min)	Endothermic temperature (°C)	Percentage weight loss	Enthalpy change (kJ/mol)
Fe_3O_4 nanoparticles	6	586	4.6	2.2
	8	594	4.4	3.57
	10	600	5.6	6.64

The activation energy of the magnetite nanoparticles was calculated by the Kissinger method [72-74] using maxima of the endothermic peaks of DTA curves at 6, 8 and 10˚C/min respectively. The Kissinger equation is as follows:

$$ln\frac{\alpha}{T_P^2} = \frac{-E_c}{RT_P} + Constant \qquad (4)$$

Where T_P is the decomposition peak temperature, α is the heating rate and R is the gas constant. A linear relationship between ln α/T_P^2 and $1000\times1/T_p$ for the maxima of the endothermic peaks was obtained using equation (4) and then the activation energy required for the decomposition reaction was calculated.

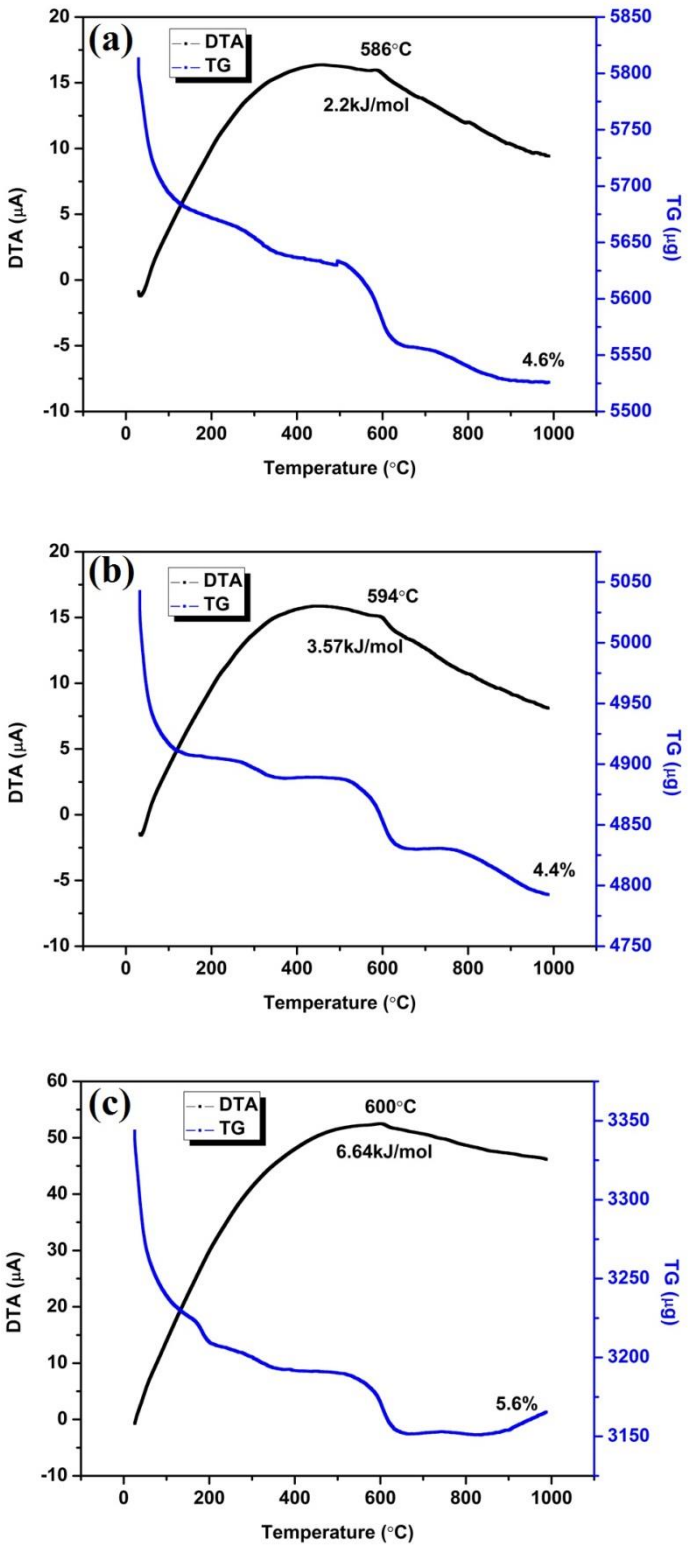

Figure 7. TG and DTA curve of green synthesized Fe_3O_4 nanoparticles at **(a)** 6˚C/minute **(b)** 8˚C/minute and **(c)** 10˚C/minute heating rates respectively

The Kissinger plot of the activation energy of the magnetite nanoparticles prepared from the *Crocus Sativus* (Saffron) flower extract is shown in figure 8. The activation energy required for the decomposition reaction was found to 8.09 kJ/moles. The calculated values of activation energy using the Kissinger method is tabulated in table 2.

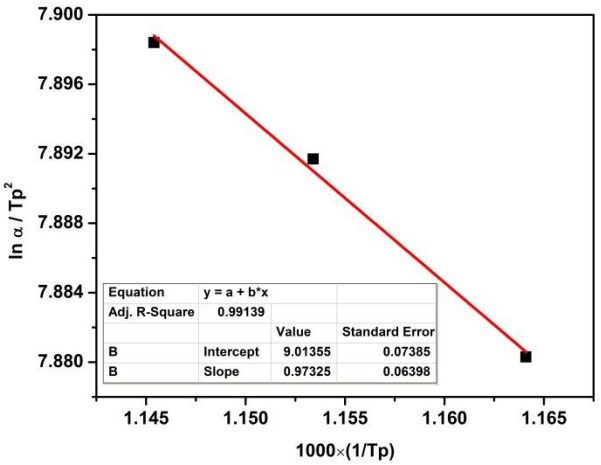

Figure 8. Kissinger plot to calculate the activation energy of green synthesized Fe_3O_4 nanoparticles.

Table 2. The calculated values of the activation energy of Fe_3O_4 nanoparticles using the Kissinger method.

Type of nanomaterial	Heating rate α (K/min)	Peak temperature T_P (K)	$\frac{\alpha}{T_P 2}$ (X 10^{-4})	$\ln\frac{\alpha}{T_P 2}$	$1000X\frac{1}{T_P}$	Activation energy E_a (kJ/mol)
Fe_3O_4 nanoparticles	279	859	3.78	-7.88	1.164	8.09
	281	867	3.74	-7.891	1.153	
	283	873	3.71	-7.898	1.145	

3.5. Antibacterial activity.

Six bacterial strains namely *Bacillus subtilis, Enterococcus faecalis, Escherichia coli, Pseudomonas aeruginosa, Salmonella enteridis, Staphylococcus aureus* were examined to study the antibacterial characteristics of Fe_3O_4 nanoparticles prepared from *Crocus Sativus* (Saffron) flower extract using MIC and MBC assays. The prepared Fe_3O_4 nanoparticles show an antibacterial effect against *E. coli* and *P. aeruginosa* at 5 mg/mL concentration as shown in figure 9.

The prepared magnetite nanoparticles give rise to the intracellular reactive oxygen concentration that urges the bacterial damage. Many researchers have published similar kind of results and they reported the potential application of Fe_3O_4 nanoparticles as a good antibacterial material. Abbasi *et al.* [75] have studied the antibacterial effect of Fe_3O_4 nanoparticles treated *Rhamnus Virgate* against some bacteria strain. They showed that Fe_3O_4 nanoparticles created an inhibitory zone against *E. coli* and *P. aeruginosa.* Vasantharaj *et al.* [76] biosynthesized magnetite nanoparticles from *Ruellia tuberose* and showed their antimicrobial properties against gram-positive and gram-negative bacteria strains. Very recently, Vitta *et al.* [77] prepared Fe_3O_4 nanoparticles from *Eucalyptus robusta* and investigated their antibacterial activity against *B. subtilis, E. coli, P. aeruginosa* and *S. aureus*. They reported that magnetite nanoparticles had shown the antibacterial activity against all tested bacteria.

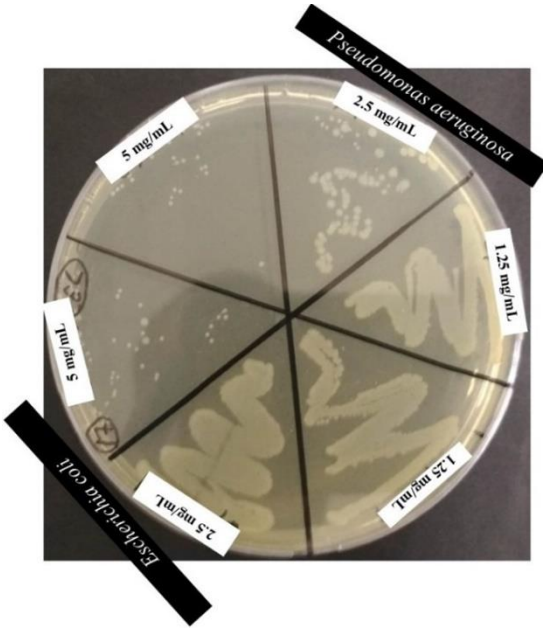

Figure 9. The antibacterial effect of prepared Fe_3O_4 nanoparticles at 5 mg/mL concentration.

The nanoparticle size and metal ions in its content have readily penetrated the cell through the pores in the cell membrane. Upon entering into the cell, they can interact with organelles, enzymes, and proteins, such as vital components for the cell. These potential intercellular interactions of nanoparticles may cause problems such as DNA replication, inactivation of enzymes, tearing of the cell wall of bacteria and cutting of the bacterial body. Since the peptidoglycan layer in the cell membrane of gram-negative bacteria is thinner than that of gram-positive, Fe_3O_4 nanoparticles may have shown antibacterial activity against gram-negative bacteria strains like current study. Therefore, Fe_3O_4 nanoparticles have been proved to inhibit bacterial growth and they are considered to be an essential factor when used appropriately.

4. CONCLUSIONS

In the present paper, we have successfully prepared Fe_3O_4 nanoparticles by a simple and environmentally friendly method using *Crocus Sativus* (Saffron) flower extract. The prepared Fe_3O_4 nanoparticles showed a single-phase cubic structure with an average crystallite size of 15 nm and a lattice strain of 0.29 as calculated from the Scherrer and Williamson-Hall equations respectively. The microstructural studies had revealed the spherical nature of the prepared magnetite nanoparticles with less agglomeration. The EDS analysis confirmed the 50:50 stoichiometric ratios of iron and oxygen theoretically and experimentally. UV-Visible spectroscopy of magnetite nanoparticles showed an absorption peak at 385 nm. The iron oxide nanoparticles showed less bandgap (3.23 eV) than other published reports; therefore they are more conductive. The prepared iron oxide nanoparticles exhibited significant stability and it was confirmed by thermogravimetric analysis due to the less weight loss over a temperature range of 30-1000 ˚C. The DTA analysis showed the endothermic peaks at 586, 594 and 600 ˚C respectively overheating rates of 6, 8 and 10˚C/min. DTA analysis confirms the shift of decomposition/endothermic peak towards higher temperatures due to the variation of enthalpy change. The enthalpy change of prepared magnetite nanoparticles at 6, 8 and 10˚C/min was found to be 2.2, 3.57 and 6.64 kJ/mol respectively. The activation energy of the prepared iron oxide nanoparticles was calculated using the Kissinger method and the value was found to be 8.09 kJ/moles. We also successfully investigated the

antibacterial activity of the prepared magnetite nanoparticles against *Bacillus subtilis*, *Enterococcus faecalis*, *Escherichia coli*, *Pseudomonas aeruginosa*, *Salmonella enteridis*, *Staphylococcus aureus* by using the MIC method. The magnetite nanoparticles showed excellent antibacterial activity against only gram-negative bacterial strains like *E. coli* and *P. aeruginosa* at 5 mg/mL concentration.

5. REFERENCES

1. Farma, R.; Deraman, M.; Awitdrus.; Talib, I.A.; Omar, R.; Manjunatha, J.G.; Ishak, M.M.; Basri, N.H.; Dolah, B.N.M. Physical and Electrochemical Properties of Supercapacitor Electrodes Derived from Carbon Nanotube and Biomass Carbon. *Int J Electrochem Sci* **2013**, *8*, 257–273.
2. Manjunatha, J.G.; Swamy, B.E.K.; Mamatha, G.P.; Gilbert, O.; Srinivas, M.T.; Sherigara, B.S. Electrochemical Studies of Clozapine Drug Using Carbon Nanotube-SDS Modified Carbon Paste Electrode: A Cyclic Voltammetry Study. *Der Pharma Chemica* **2011**, *3*, 236-249.
3. Tigari, G.; Manjunatha, J.G.; Raril, C.; Hareesh, N. Determination of Riboflavin at Carbon Nanotube Paste Electrodes Modified with an Anionic Surfactant. *ChemistrySelect* **2019**, *4*, 2168–2173, https://doi.org/10.1002/slct.201803191.
4. Shashanka, R.; Chaira, D.; Swamy, B.E.K. Fabrication of yttria dispersed duplex stainless steel electrode to determine dopamine, ascorbic and uric acid electrochemically by using cyclic voltammetry. *International Journal of Scientific & Engineering Research* **2016**, *7*, 1275-1285.
5. Tigari, G.; Manjunatha, J.G.; Raril, C.; Hareesha, N. Electrochemical Determination of Resorcinol with Tartrazine at Non-Ionic Surfactant Modified Graphite Powder and Carbon Nanotube Composite Paste Electrode. *Nov Appro Drug Des Dev* **2019**, *4*.
6. Charithra, M.M.; Manjunatha, J.G. Enhanced voltammetric detection of paracetamol by using carbon nanotube modified electrode as an electrochemical sensor. *J Electrochem Sci Eng* **2020**, *10*, 29-40, http://dx.doi.org/10.5599/jese.717.
7. Benelmekki, M. An introduction to nanoparticles and nanotechnology, Designing Hybrid Nanoparticles. *IOP Concise Physics, Morgan & Claypool Publishers* **2015**, https://doi.org/10.1088/978-1-6270-5469-0ch1.
8. Shashanka, R. Synthesis of nano-structured stainless steel powder by mechanical alloying-an overview. *International Journal of Scientific & Engineering Research* **2017**, *8*, 588–594.
9. Kung, H.H. Transition Metal Oxides: Surface Chemistry and Catalysis. *Elsevier*. Amsterdam; **1989**.
10. Mahdavian, A.R.; Mirrahimi, M.A.S. Efficient separation of heavy metal cations by anchoring polyacrylic acid on superparamagnetic magnetite nanoparticles through surface modification. *Chem Eng J* **2010**, *159*, 264–271, https://doi.org/10.1016/j.cej.2010.02.041.
11. Hu, F.Q.; Wei, L.; Zhou, Z.; Ran, Y.L.; Li, Z.; Gao, M.Y. Preparation of biocompatible magnetite nanocrystals for in vivo magnetic resonance detection of cancer. *Adv Mater* **2006**, *18*, 2553–2556, https://doi.org/10.1002/adma.200600385.
12. Zhao, H.; Saatchi, K.; Häfeli, U.O. Preparation of biodegradable magnetic microspheres with poly(lactic acid)-coated magnetite. *J Magn Magn Mater* **2009**, *321*, 1356–1363, https://doi.org/10.1016/j.jmmm.2009.02.038.
13. Zhang, L.; Dong, W.F.; Sun, H.B. Multifunctional superparamagnetic iron oxide nanoparticles: design, synthesis and biomedical photonic applications. *Nanoscale* **2013**, *5*, 7664–7684, https://doi.org/10.1039/c3nr01616a.
14. Gawande, M.B.; Branco, P.S.; Varma, R.S. Nano-magnetite (Fe_3O_4) as a support for recyclable catalysts in the development of sustainable methodologies. *Chem Soc Rev* **2013**, *42*, 3371–3393, https://doi.org/10.1039/C3CS35480F.
15. Sharad, N.S.; Swapnil, R.B.; Ganesh, R.M.; Samadhan, S.K.; Dinesh, K.M.; Shashikant, B.B.; Rathi, A.K.; Bundaleski, N.; Teodoro, O.M.N.D.; Zboril, R.; Varma, R.S.; Gawande, M.B. Iron oxide-supported copper oxide nanoparticles (nanocat-Fe-CuO): magnetically recyclable catalysts for the synthesis of pyrazole derivatives, 4-methoxyaniline, and ullmann-type condensation reactions. *ACS Sustainable Chem Eng* **2014**, *2*, 1699–1706, https://doi.org/10.1021/sc500160f.
16. Wong, E.W.; Bronikowski, M.J.; Hoenk, M.E.; Kowalczyk, R.S.; Hunt, B.D. Submicron patterning of iron nanoparticle monolayers for carbon nanotube growth. *Chem Mater* **2005**, *17*, 237-241, https://doi.org/10.1021/cm048795m.
17. Terris, B.D.; Thomson, T. Nanofabricated and self-assembled magnetic structures as data storage media. *J Phys D Appl Phys* **2005**, *38*, R199–R222.
18. Kavitha, A.L.; Prabu, H.G.; Babu, S.A.; Suja, S.K. Magnetite nanoparticles chitosan composite containing carbon paste electrode for glucose biosensor application. *J Nanosci Nanotechnol* **2013**, *13*, 98–104, https://doi.org/10.1166/jnn.2013.6720.
19. Chaki, S.H.; Malek, T.J.; Chaudhary, M.D.; Tailor, J.P.; Deshpande, M.P. Magnetite Fe_3O_4 nanoparticles synthesis by wet chemical reduction and their characterization. *Adv Nat Sci: Nanosci Nanotechnol* **2015**, *6*, https://doi.org/10.1088/2043-6262/6/3/035009.
20. Jun, Y.W.; Huh, Y.M.; Choi, J.S.; Lee, J.H.; Song, H.T.; KimKim.; Yoon, S.; Kim, K.S.; Shin, J.S.; Suh, J.S.; Cheon, J. Nanoscale size effect of magnetic nanocrystals and their utilization for cancer diagnosis via magnetic resonance imaging. *J Am Chem Soc* **2005**, *127*, 5732-5733, https://doi.org/10.1021/ja0422155.
21. Li, F.; Vipulanandan, C.; Mohanty, K.K. Microemulsion and solution approaches to nanoparticle iron production for degradation of trichloroethylene. *Colloids and Surfaces A: Physicochem Eng Aspects* **2003**, *223*, 103-112, https://doi.org/10.1016/S0927-7757(03)00187-0.
22. Salem, M.; Xia, Y.; Allan, A.; Rohani, S.; Gillies, E.R. Curcumin-loaded, folic acid-functionalized magnetite particles for targeted drug delivery. *RSC Adv* **2015**, *5*, 37521–37532, https://doi.org/10.1039/c5ra01811k.
23. Li, X.; Li, H.; Liu, G.; Deng, Z.; Wu, S.; Li, P.; Xu, Z.; Xu, H.; Chu, P.K. Magnetite-loaded fluorine-containing polymeric micelles for magnetic resonance imaging and drug delivery. *Biomaterials* **2012**, 33, 3013–3024, https://doi.org/10.1016/j.biomaterials.2011.12.042.
24. Wani, K.D.; Kadu, B.S.; Mansara, P.; Gupta, P.; Deore, A.V.; Chikate, R.C.; Poddar, P.; Dhole, S.D.; Ruchika K.G. Synthesis, characterization and in vitro study of biocompatible cinnamaldehyde functionalized magnetite nanoparticles (CPGF Nps) for hyperthermia and drug delivery applications in breast cancer. *PLoS One* **2014**, *9*, e107315, https://doi.org/10.1371/journal.pone.0107315.
25. Zhang, W.X. Nanoscale Iron Particles for Environmental Remediation: An Overview. *J Nanopart Res* **2003**, *5*, 323–332, https://doi.org/10.1023/A:1025520116015.

26. Blaney, L. Magnetite (Fe_3O_4): Properties, Synthesis, and Applications. *Lehigh review* **2007**, *15*, 33–81.
27. Fried, T.; Shemer, G.; Markovich, G. Ordered two dimensional arrays of ferrite nanoparticles. *Adv Mater* **2001**, *13*, 1158–1561, https://doi.org/10.1002/1521-4095(200108)13:15<1158::AID-ADMA1158>3.0.CO;2-6.
28. Tang, J.; Myers, M.; Bosnick, K.A.; Brus, L.E. Magnetite Fe_3O_4 nanocrystals: spectroscopic observation of aqueous oxidation kinetics. *J Phys Chem B* **2003**, *107*, 7501–7506, https://doi.org/10.1021/jp027048e.
29. Zhou, Z.H.; Wang, J.; Liu, X.; Chan, H.S.O. Synthesis of Fe_3O_4 nanoparticles from emulsions. *J Mater Chem* **2001**, *11*, 1704–1709, https://doi.org/10.1039/B100758K.
30. Breulmann, M.; Colfen, H.; Hentze, H.P.; Antonietti, M.; Walsh, D.; Mann, S. Elastic magnets: template-controlled mineralization of iron oxide colloids in a sponge-like gel matrix. *Adv Mater* **1998**, *10*, 237–241, https://doi.org/10.1002/(SICI)1521-4095(199802)10:3<237::AID-ADMA237>3.0.CO;2-6.
31. Morais, P.C.; Garg, V.K.; Oliveira, A.C.; Azevedo, R.B.; Rabelo, D.; Lima, E.C.D. Synthesis and characterization of magnetite nanoparticles embedded in copolymer microspheres. *eCells & Materials* **2002**, *3*, 173–175.
32. Venkatesan, M.; Nawka, S.; Pillai, S.C.; Coey, J.M.D. Enhanced magnetoresistance in nanocrystalline magnetite. *Appl Phys* **2003**, *93*, 8023–8025, https://doi.org/10.1063/1.1555371.
33. Xu, J.; Yang, H.; Fu, W.; Du, K.; Sui, Y.; Chen, J.; Zeng, Y.; Li, M.; Zou, G. Preparation and magnetic properties of magnetite nanoparticles by sol–gel method. *J Magn Magn Mater* **2007**, *309*, 307–311, https://doi.org/10.1016/j.jmmm.2006.07.037.
34. Cabrera, L.; Gutierrez, S.; Menendez, N.; Morales, P.; Herrasti, P. Magnetite nanoparticles: Electrochemical synthesis and characterization. *Electrochim Acta* **2008**, *53*, 3436–3441, https://doi.org/10.1016/j.electacta.2007.12.006.
35. Liu, X.M.; Kim, J.K. Solvothermal synthesis and magnetic properties of magnetite nanoplatelets. *Mater Lett* **2009**, *63*, 428–430, https://doi.org/10.1016/j.matlet.2008.11.001.
36. Zhang, Z.J.; Chen, X.Y.; Wang, B.N.; Shi, C.W. Hydrothermal synthesis and self-assembly of magnetite (Fe_3O_4) nanoparticles with the magnetic and electrochemical properties. *J Cryst Growth* **2008**, *310*, 5453–5457, https://doi.org/10.1016/j.jcrysgro.2008.08.064.
37. Shashanka, R.; Karaoglanli, A.C.; Ceylan, Y.; Uzun, O. A fast and robust approach for the green synthesis of spherical Magnetite (Fe_3O_4) nanoparticles by Tilia Tomentosa (Ihlamur) leaves and its antibacterial studies. *Pharmaceutical Sciences* **2020**.
38. Crocus Sativus, Germplasm Resources Information Network (GRIN). Agricultural Research Service (ARS). *United States Department of Agriculture (USDA)* Retrieved 23 April **2015**.
39. Kafi, M.; Koocheki, A.; Rashed, M.H.; Nassiri, M. *Saffron (Crocus Sativus) Production and Processing.* 1st ed. Science Publishers 2006.
40. Schmidt, T.; Heitkam, T.; Liedtke, S.; Schubert, V.; Menzel, G. Adding color to a century-old enigma: multi-color chromosome identification unravels the autotriploid nature of saffron (Crocus Sativus) as a hybrid of wild Crocus cartwrightianus cytotypes. *New Phytologist* **2019**, *222*, 1965–1980, https://doi.org/10.1111/nph.15715.
41. Nemati, Z.; Blattner, F.R.; Kerndorff, H.; Erol, O.; Harpke, D. Phylogeny of the saffron-crocus species group, Crocus series Crocus (Iridaceae). *Molecular Phylogenetics and Evolution* **2018**, *127*, 891–897, https://doi.org/10.1016/j.ympev.2018.06.036.
42. Bowles, E.A. *A Handbook of Crocus and Colchicum for Gardeners*. Van Nostrand, Toronto; 1952.
43. Clarina, T.; Flomina, P.J.; Thangeswari, P.; Rama, V. Polpala Flower Extract Mediated One Step Green Synthesis and Characterization of Magnetite (Fe_3O_4) Nanoparticles. *Asian J Research Chem* **2018**, *11*, 459-462, https://doi.org/10.5958/0974-4150.2018.00083.4.
44. Karpagavinayagam, P.; Vedhi, C. Green synthesis of iron oxide nanoparticles using Avicennia marina flower extract. *Vacuum* **2019**, *160*, 286–292, https://doi.org/10.1016/j.vacuum.2018.11.043.
45. Sari, I.P.; Yulizar, Y. Green synthesis of magnetite (Fe_3O_4) nanoparticles using Graptophyllum pictum leaf aqueous extract. *IOP Conf Series: Materials Science and Engineering* **2017**, *191*, https://doi.org/10.1088/1757-899X/191/1/012014.
46. Ramesh, A.V.; Devi, D.R.; Botsa, S.M.; Basavaiah, K. Facile green synthesis of Fe_3O_4 nanoparticles using aqueous leaf extract of Zanthoxylum armatum DC. for efficient adsorption of methylene blue. *Journal of Asian Ceramic Societies* **2018**, *6*, 145-155, https://doi.org/10.1080/21870764.2018.1459335.
47. Doble, M.; Kruthiventi, A.K. *Green chemistry and engineering.* 1st ed. *Academic Press* **2007**.
48. Esmaeili, N.; Ebrahimzadeh, H.; Abdi, K.; Safarian, S. Determination of some phenolic compounds in Crocus Sativus L. corms and its antioxidant activities study. *Pharmacogn Mag* **2011**, *7*, 74–80, https://doi.org/10.4103/0973-1296.75906.
49. Karimi, E.; Oskoueian, E.; Hendra, R.; Jaafar, H.Z.E. Evaluation of Crocus Sativus L. Stigma Phenolic and Flavonoid, Compounds and Its Antioxidant Activity. *Molecules* **2010**, *15*, 6244-6256, https://doi.org/10.3390/molecules15096244.
50. Siddhuraju, P.; Becker, K. Antioxidant properties of various solvent extracts of total phenolic constituents from three different agroclimatic origins of drumstick tree (Moringa oleifera Lam.) leaves. *J Agric Food Chem* **2003**, *51*, 2144-2155, https://doi.org/10.1021/jf020444.
51. Andrews, J.M. Determination of minimum inhibitory concentraitons. *J Antimicrob Chemother* **2002**, *49*, 1049-1050, https://doi.org/10.1093/jac/48.suppl_1.5.
52. Shashanka, R.; Chaira, D. Phase transformation and microstructure study of nano-structured austenitic and ferritic stainless steel powders prepared by planetary milling. *Powder Technol* **2014**, *259*, 125–136, https://doi.org/10.1016/j.powtec.2014.03.061.
53. Reddy, S.; Swamy, B.E.K.; Aruna, S.; Kumar, M.; Shashanka, R.; Jayadevappa, H. Preparation of NiO/ZnO hybrid nanoparticles for electrochemical sensing of dopamine and uric acid. *Chem Sensors* **2012**, *2*, 1–7.
54. Aparna, Y.; Rao, V.K.; Subbarao, P.S. Preparation and Characterization of CuO Nanoparticles by Novel Sol-Gel Technique. *J Nano-Electron Phys* **2012**, *4*, 03005.
55. Shashanka, R.; Chaira, D. Optimization of milling parameters for the synthesis of nano-structured duplex and ferritic stainless steel powders by high energy planetary milling. *Powder Technol* **2015**, *278*, 35–45, https://doi.org/10.1016/j.powtec.2015.03.007.
56. Shashanka, R.; Chaira, D.; Swamy, B.E.K. Electrochemical investigation of duplex stainless steel at carbon paste electrode and its application to the detection of dopamine, ascorbic and uric acid. *International Journal of Scientific & Engineering Research* **2015**, *6*, 1863–1871.
57. Shashanka, R. Effect of Sintering Temperature on the Pitting Corrosion of Ball Milled Duplex Stainless Steel by using Linear Sweep Voltammetry. *Anal Bioanal Electrochem* **2018**, *10*, 349-361.
58. Shashanka, R.; Chaira, D.; Swamy, B.E.K. Electrocatalytic Response of Duplex and Yittria Dispersed Duplex Stainless Steel Modified Carbon Paste Electrode in Detecting Folic Acid Using Cyclic Voltammetry. *Int J Electrochem Sci* **2015**, *10*, 5586–5598.
59. Nayak, A.K.; Shashanka, R.; Chaira, D. Effect of Nanosize Yittria and Tungsten Addition to Duplex Stainless Steel During

High Energy Planetary Milling. *IOP Conf Ser Mater Sci Eng* **2016**, *115*, https://doi.org/10.1088/1757-899X/115/1/012008.
60. Gupta, S.; Shashanka, R.; Chaira, D. Synthesis of nano-structured duplex and ferritic stainless steel powders by planetary milling: An experimental and simulation study. *IOP Conf Ser Mater Sci Eng* **2015**, *75*, https://doi.org/10.1088/1757-899X/75/1/012033.
61. Shashanka, R.; Swamy, B.E.K. Biosynthesis of silver nanoparticles using leaves of Acacia melanoxylon and its application as dopamine and hydrogen peroxide sensors. *Physical Chemistry Research* **2020**, *8*, 1-18.
62. Moustafa, M.H.; Al Din, R.S. Green synthesis and characterization of iron-oxide nanoparticles by guava aqueous leaves extract for doxorubicin drug loading. *J Biosci Appl Res* **2017**, *3*, 177–180.
63. Dharma, J.; Pisal, A. *Application Note, UV/Vis/NIR Spectrometer*. PerkinElmer, Inc. 940 Winter Street, Waltham. MA 02451. USA.
64. El Ghandoor, H.; Zidan, H.M.; Khalil, M.M.H, Ismail MIM. Synthesis and Some Physical Properties of Magnetite (Fe_3O_4) Nanoparticles. *Int J Electrochem Sci* **2012**, *7*, 5734–5745.
65. El-Diasty, F.; El-Sayed, H.M.; El-Hosiny, F.I.; Ismail, M.I.M. Complex susceptibility analysis of magneto-fluids: Optical band gap and surface studies on the nanomagnetite-based particles. *Curr Opin Solid State Mater Sci* **2009**, *13*, 28–34, https://doi.org/10.1016/j.cossms.2008.09.002.
66. Salunkhe, A.B.; Khot, V.M.; Ruso, J.M.; Patil, S.I. Synthesis and magnetostructural studies of amine functionalized superparamagnetic iron oxide nanoparticles. *RSC Adv* **2015**, *5*, 18420–18428, https://doi.org/10.1039/c5ra00049a.
67. Shashanka, R.; Swamy, B.E.K.; Reddy, S.; Chaira, D. Synthesis of Silver Nanoparticles and their Applications. *Anal Bioanal Electrochem* **2013**, *5*, 455–466.
68. Mahdavi, M.; Ahmad, M.B.; Haron, M.J.; Namvar, F.; Nadi, B.; Ab Rahman, M.Z.; Amin, J. Synthesis, Surface Modification and Characterisation of Biocompatible Magnetic Iron Oxide Nanoparticles for Biomedical Applications. *Molecules* **2013**, *18*, 7533-7548, https://doi.org/10.3390/molecules18077533.
69. Zhao, S.Y.; Lee, D.G.; Kim, C.W.; Cha, H.G.; Kim, Y.H.; Kang, Y.S. Synthesis of magnetic nanoparticles of Fe_3O_4 and $CoFe_2O_4$ and their surface modification by surfactant adsorption. *Bull Korean Chem Soc* **2006**, *27*, 237–242, https://doi.org/10.5012/bkcs.2006.27.2.237.
70. Manjari, G.; Saran, S.; Arun, T.; Rao, A.V.B.; Devipriya, S.P. Catalytic and recyclability properties of phytogenic copper oxide nanoparticles derived from Aglaia elaeagnoidea flower extract. *Journal of Saudi Chemical Society* **2017**, *21*, 610–618, https://doi.org/10.1016/j.jscs.2017.02.004.
71. Chrostek, T. Chapter 6-The influence of the heating and cooling rates on the temperature of the phase transitions. *Oficyna Wydawnicza Stowarzyszenia Menedżerów Jakości i Produkcji* **2016**.
72. Wang, Z.J.; Ni, W.; Jia, Y.; Zhu, L.P.; Huang, X-Y. Crystallization behavior of glass ceramics prepared from the mixture of nickel slag, blast furnace slag and quartz sand. *Journal of Non-Crystalline Solids* **2010**, *356*, 1554–1558, https://doi.org/10.1016/j.jnoncrysol.2010.05.063.
73. Kissinger, H.E. Variation of Peak Temperature With Heating Rate in Differential Thermal Analysis. *J Res Natl Bur Stand* **1956**, *57*, 217–221.
74. Shashanka, R.; Chaira, D. Development of nano-structured duplex and ferritic stainless steel by pulverisette planetary milling followed by pressureless sintering. *Mater Charact* **2015**, *99*, 220-229, https://doi.org/10.1016/j.matchar.2014.11.030.
75. Abbasi, B.A.; Iqbal, J.; Mahmood, T.; Qyyum, A.; Kanwal, S. Biofabrication of iron oxide nanoparticles by leaf extract of Rhamnus virgata: Characterization and evaluation of antimicrobial and antioxidant potentials. *Appl Organometal Chem* **2019**, *33*, 1-15, https://doi.org/10.1002/aoc.4947.
76. Vasantharaj, S.; Sathiyavimal, S.; Senthilkumar, P.; LewisOscar, F.; Pugazhendhi, A. Biosynthesis of iron oxide nanoparticles using leaf extract of Ruellia tuberosa: antimicrobial properties and their applications in photocatalytic degradation. *Journal of Photochemistry and Photobiology B: Biology* **2019**, *192*, 74-82, https://doi.org/10.1016/j.jphotobiol.2018.12.025
77. Vitta, Y.; Figueroa, M.; Calderon, M.; Ciangherotti, C. Synthesis of iron nanoparticles from aqueous extract of Eucalyptus robusta Sm and evaluation of antioxidant and antimicrobial activity. *Materials Science for Energy Technologies* **2020**, *3*, 97-103, https://doi.org/10.1016/j.mset.2019.10.014.

6. ACKNOWLEDGEMENTS

The authors gratefully acknowledge Bartin University Scientific Research Projects Unit, Turkey for providing financial support to conduct the research (Project number: 2019-FENA-006).